Available online at www.sciencedirect.com
ScienceDirect
Journal of the European Ceramic Society 27 (2007) 2567–2576
www.elsevier.com/locate/jeurceramsoc

# Size effect in low grain size neodymium doped PZT ceramics

Uta Helbig *

*Fraunhofer-Institut für Silicatforschung, Würzburg, Germany*

Received 2 June 2006; received in revised form 12 September 2006; accepted 24 September 2006
Available online 5 January 2007

**Abstract**

Low grain size neodymium doped lead zirconate titanate ceramics (PZT) were synthesised via a sol–gel method. The phase content, the crystal structure and the dielectric and ferroelectric properties were investigated in dependence of the microstructure and the zirconium/titanium ratio. The aim of the work was the investigation of the correlation between microstructure and properties at very low grain sizes.

Below a critical grain size of 1 μm a significant change of the properties and the phase content was observed. The morphotropic phase boundary shifts towards titanium-rich compositions. The experimental observations were compared with model calculations based on the Devonshire theory concerning the room temperature stability of the rhombohedral and tetragonal phase and the position of the morphotropic phase boundary.


*Keywords:* Grain size; X-ray methods; Dielectric properties; Ferroelectric properties; PZT

## 1. Introduction

Lead zirconate titanate (PZT) ceramics are a common material for piezoelectric sensors and actuators. Despite some disadvantages of the material like brittleness, low impedance matching and the toxicity of educts, the material is one of the most prominent ferroelectric ceramics because of its excellent piezoelectric properties. The temperature stability, coupling coefficients and mechanical forces exceed those of other piezoelectric materials like polymer foils by far.

The material has been studied intensively since the discovery of the miscibility of lead titanate and lead zirconate in the 1950s. The excellent properties are related to the existence of the morphotropic phase boundary (MPB) between the tetragonal and the rhombohedral phase. The position of the phase boundary and its thermodynamic background were the subject of numerous studies.[1–9] The phase boundary was found to be a coexistence region with a width dependent on the process parameters.[2,3,7,10] Härdtl and Hennings[10] compared the width of the morphotropic phase boundary of ceramics with varied densities and observed a broadening of the coexistence region in PZT ceramics sintered to full density. By contrast, recent investigations of Kim[11] revealed no influence of the microstructure on the width of the phase boundary. These discrepancies in the results indicate that the problem has not yet been fully understood. Additionally, new fabrication methods lead to extremely fine grained material[12–17] so that the investigations have to be extended towards lower grain sizes.

The properties of lead zirconate titanate ceramics can be adjusted by the introduction of dopant ions. The dopants influence the ferroelectric properties, so-called 'hard-' and 'soft-'doped material can be fabricated matching the application. Beside the influence on the ferroelectric properties, the dopants alter the sinterability of the ceramic. Several studies were carried out concerning this topic.[18–21] The dopant ions are supposed to enrich at the grain boundaries and reduce the grain growth of the material.

Within that context, the correlation between microstructure and material properties was intensively studied by several groups.[22–26] It was shown that the remanent polarisation, the piezoelectric coefficients and the coupling factors decrease with decreasing grain size of the ceramic.[22–26] If additional phases at the grain boundaries can be excluded, the reasons for the drop of the properties are space charges[25] and mechanical stress.[23,24] The mechanical stress has an effect on the crystal lattice which was proved by Randall et al.[25]

In this study, the correlation between the morphotropic phase boundary and the grain size of neodymium doped PZT ceramics is investigated. The ceramic material was fabricated after a

* Correspondence address: Lehrstuhl für Chemische Technologie der Materialsynthese, Universität Würzburg, Röntgenring 11, D-97070 Würzburg, Germany. Tel.: +49 931 312157; fax: +49 931 312109.
*E-mail address:* uta.helbig@matsyn.uni-wuerzburg.de.

0955-2219/$ – see front matter © 2006 Elsevier Ltd. All rights reserved.
doi:10.1016/j.jeurceramsoc.2006.09.018

sol–gel method developed for the synthesis of fine scaled PZT fibres.[15–17]

The samples were investigated with respect to microstructure, dielectric properties and phase content. These data are compared to model calculations using the Devonshire theory.

This method was developed for barium titanate by Devonshire in the 1940s and has enabled a full theoretical description of the material for the first time. Based on the polarisation as the ordering parameter, the phase transitions of barium titanate could be calculated.

Later on, the theory was extended to the solid solution system lead zirconate–lead titanate.[27–31] Based on material data determined from sol–gel PZT ceramics, the calculation of the complete phase diagram of PZT became possible.[32] A full set of material coefficients was determined by Haun et al.[33–36]

Based on these data, several groups were able to calculate the influence of mechanical parameters like hydrostatic pressure on the phase transition points of PZT, i.e. the Curie temperature and the morphotropic phase boundary between the tetragonal and the rhombohedral phases.[37–39]

## 2. Experimental

For the investigation of the microstructure effects, ceramic pellets of neodymium doped PZT were synthesised. A sol–gel method was used for the preparation of the samples.[15–17]

The sol (scheduled quantity 1 mol) was synthesised by mixing titaniumethylate and zirconiumpropylate (Tyzor® ET, DuPont™) in the molar ratio corresponding to the PNdZT composition. The alcoholates were carboxylated by the addition of 0.5 mol capronic acid (Fluka) and stirring for 10 min and subsequent addition of 3.5 mol propionic acid (Sigma–Aldrich) and stirring for 30 min. The water emerging from esterification enables the controlled hydrolysis without the addition of water. Subsequently, lead oxide (Alfa Aesar) and neodymium acetate hydrate (Sigma–Aldrich) were added. Refluxation at 120 °C for 2 h and concentration to about 60 wt.% solids content provides a storable solid precursor.

The precursor powder was dried for 1 week at 50 °C and 1 week at 110 °C. The dried powder was heated to 300 °C within 12 h under nitrogen and to 600 °C within 12 h in air to pyrolyse the organic constituents. The resulting inorganic material was ground in an agate mortar. Related to the mass of PNdZT, a binder consisting of 34 wt.% water, 1.5 wt.% partially hydrolysed polyvinylalcohol (Mowiol® 18–88, Clariant GmbH) and 0.25 wt.% polyglycol (35000S, Clariant GmbH) was added. After thoroughly mixing and drying for 12 h at 90 °C, the material was uniaxially pressed to pellets with a diameter of 13 mm and a height of about 1 mm applying a load of 4 tonnes (corresponding to a pressure of 0.3 GPa) for 30 s. The binder was burned out in air using the following programme: heating from room temperature to 400 °C with a heating rate of 2 K/min, heating to 500 °C with a heating rate of 1 K/min, soaking 500 °C for 3 h and 20 min, cooling to room temperature with a rate of 4 K/min.

The samples were subsequently sintered in a closed alumina case. A powder mixture of 92 wt.% lead zirconate and 8 wt.% zirconia was added to prevent lead oxide loss from the samples during sintering. The pellets were placed over the powder on perforated zirconia sheets. The sintering temperature was varied between 900 °C and 1100 °C in steps of −223 °C. The heating rate was 6 K/min, the soaking time was 5 h. The samples were cooled down following the furnace characteristics.

The composition of the samples was varied between a Zr/Ti ratio 56/44 and 44/56. The neodymium content was kept constant at 2 mol%.

## 3. Characterisation

The microstructure of the samples including grain size, open and closed porosity was characterised by scanning electron microscopy (Hitachi S800), He-pycnometry (AccuPyc1330, Micromeritics GmbH) and the Archimedes method.

The porosity of the samples was investigated on polished cross sections via SEM. The images were analysed pertaining to pore volume content with the image analysis software ImageC (Imtronic GmbH). Closed porosity was determined from the skeleton density measured by He-pycnometry. As a reference the X-ray density was used which was calculated from the lattice parameters measured via powder diffraction.

The apparent densities of the whole samples were determined using the Archimedes method. The ceramic samples were infiltrated with an epoxy resin (Epofix, Struers GmbH) prior to measurement.

The grain size was determined at the surface of the samples using the lineal intercept method by digital image analysis (ImageC, Imtronic GmbH). It was verified on control samples that the grain size of the bulk is identical to that of the surface. The domain structure was depicted at polished cross sections after etching with a solution of nitric acid (7.5%) and hydrofluoric acid (0.006%) by SEM.

Dielectric constants of the ceramics were determined before poling using an impedance bridge (HP 4194A, Hewlett-Packard). Polarisation–field strength curves were measured by a four channel oscilloscope (TDS460, Tektronix). The measuring frequency was 5 Hz. The voltage was increased from 500 V to 4500 V. Prior to the investigations, the samples were infiltrated by an epoxy resin to enlarge the mechanical stability. After polishing of the surface, each side of the pellet was sputtered with a gold electrode.

The measured dielectric constants and the polarisation of the samples were recalculated by the Bruggemann formula[41] to account for the porosity using the apparent density determined by the Archimedes method.

X-ray diffraction measurements were conducted with a laboratory powder diffractometer (D5005, Siemens). The samples were measured as sintered and for comparison as a powder ground manually in an agate mortar. The step size was 0.02° and the measuring time 8 s. The diffraction data were analysed using the Rietveld method. The program used was TOPAS by Bruker AXS. The instrumental reflection broadening was determined by a $LaB_6$ standard material (NIST).

## 4. Results

### 4.1. Microstructure

In Fig. 1a and b, the mean grain size and the porosity of the sintered ceramics in terms of percentage of theoretical density are depicted. The values were determined on polished cross sections by image analysis and were averaged over all chemical compositions and plotted in dependence of the sintering temperature. As it is expected, the density of the sintered samples increases with increasing sintering temperature. The values range from about 75% theoretical density for low sintering temperatures to about 95% theoretical after sintering at 1100 °C. For the separation of open and closed porosity, He-pycnometry measurements were carried out and revealed a skeleton density of 97.6 ± 0.8% theoretical density for the samples with a sintering temperature of 900 °C and 98.4 ± 1.0% theoretical density for ceramics sintered at 1100 °C.

With enhanced sintering temperature, the mean grain size ($d_{50}$) increased from 400 nm to 1.5 μm. A correlation between chemical composition and grain size or density was not observed in accordance with the data published by Roßner.[42]

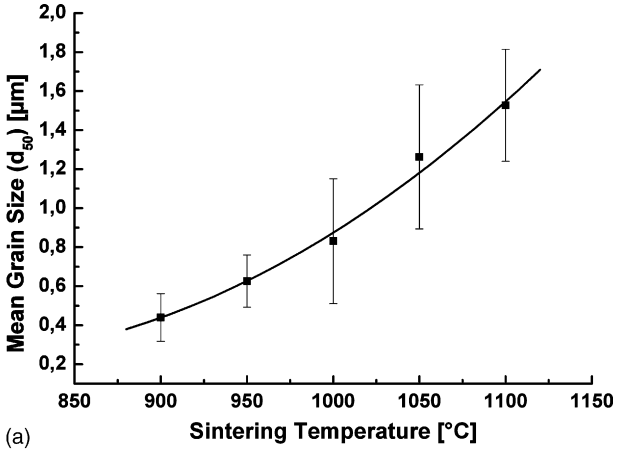


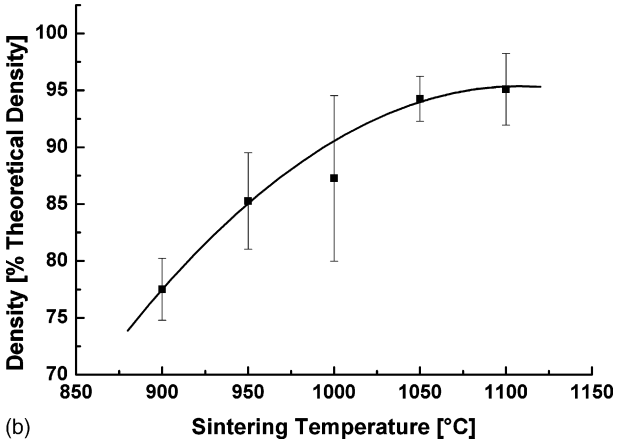


Fig. 1. (a) Mean grain size of the neodymium doped PZT ceramics vs. sintering temperature. (b) Density of the neodymium doped PZT ceramics vs. sintering temperature. Note the large error bar at 1000 °C which may be correlated with the termination of the sintering process at a maximum shrinkage rate.

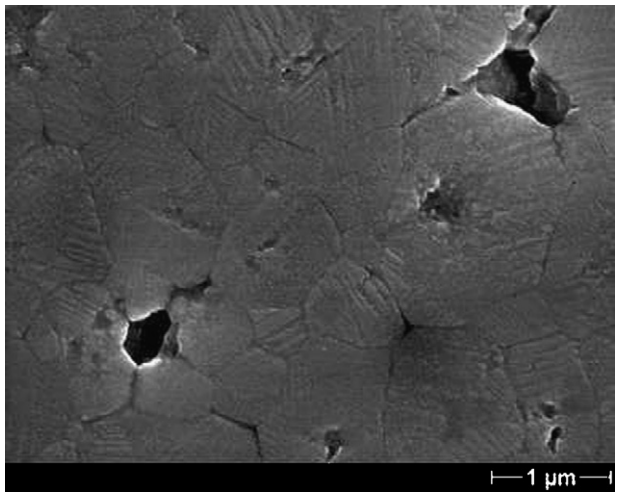


Fig. 2. Polished and subsequently etched cross section of a Nd–PZT ceramic (Zr/Ti ratio 46/54) after sintering at 1100 °C for 5 h (mean grain size 1.3 μm). The image shows the typical herringbone domain pattern of a tetragonal ceramic.

The size of the ferroelectric domains was estimated from SEM images of samples in the tetragonal composition range with a zirconium/titanium ratio of 46/54. The domain size was found to decrease with the mean grain size. The domain size at high grain sizes (1.5 μm) is around 30 nm as shown in Fig. 2. The samples with grain sizes below 1 μm show no well defined domain structures (see Fig. 3).

Samples with a composition in the rhombohedral range and at the morphotropic phase boundary did not show domain structures on etched surfaces. Beside the grain boundaries, no regular patterns could be observed in SEM (Fig. 4).

### 4.2. Dielectric and ferroelectric properties

The dielectric constant before poling determined at a sample series with high sintering temperatures, i.e. large grain sizes,

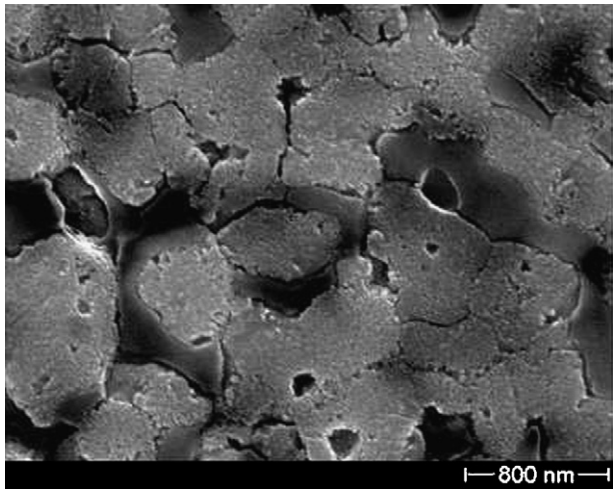


Fig. 3. Polished and subsequently etched cross section of a Nd–PZT ceramic (Zr/Ti ratio 46/54) after sintering at 900 °C for 5 h. The etch pattern reveals no distinct domain lamellae but a fine scaled granular structure.

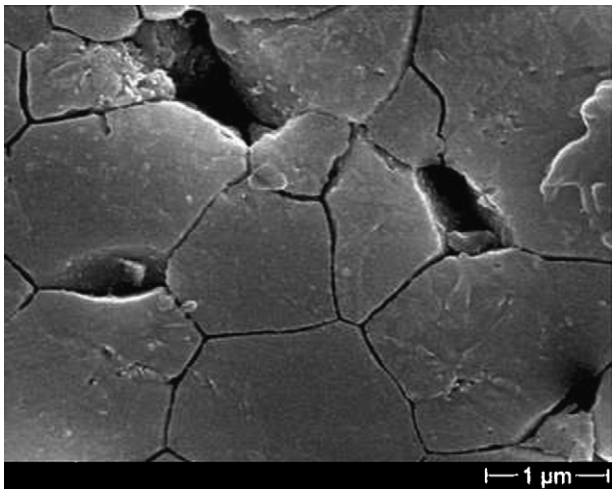


Fig. 4. Polished and subsequently etched cross section of a Nd–PZT ceramic (Zr/Ti ratio 56/44) after sintering at 1100 °C for 5 h. The composition of the sample corresponds to the morphotropic phase boundary but no domain patterns are recognisable.

was found to decrease with increasing titanium content of the ceramics (Fig. 5).

In contrast to the behaviour of the ceramics sintered at high temperatures, the material with small grain sizes shows a different behaviour (see Fig. 6). Within the range investigated, the dependence of the permittivity on the composition shows clear maxima which shift towards higher titanium contents at lower grain sizes.

As a measure for the remanent polarisation, the values for a constant electric field of 4 V/µm were compared. As shown in Fig. 7, the behaviour of the dielectric properties could be confirmed. The material with a large grain size shows a decrease of the remanent polarisation with increasing titanium content whereas the small grain size material shows a maximum in the titanium rich composition region corresponding with the dielectric properties. The remanent saturation polarisation could not be determined due to the low breakdown stability of the samples.

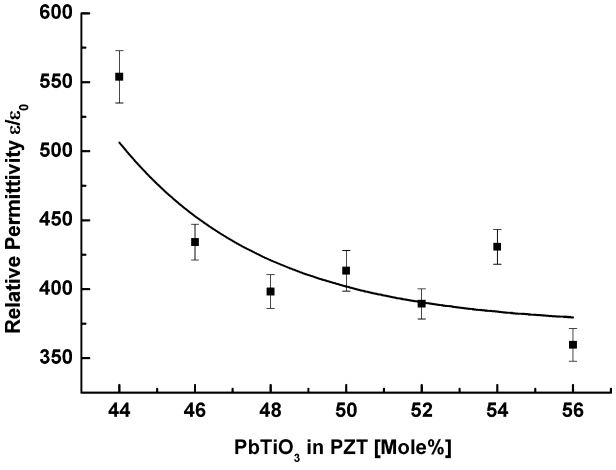


Fig. 5. Relative permittivity (unpolarised) vs. titania content of a Nd–PZT sample with a grain size of 1.3 µm. The permittivity decreases with increasing titania content due to deviation from the morphotropic phase boundary.

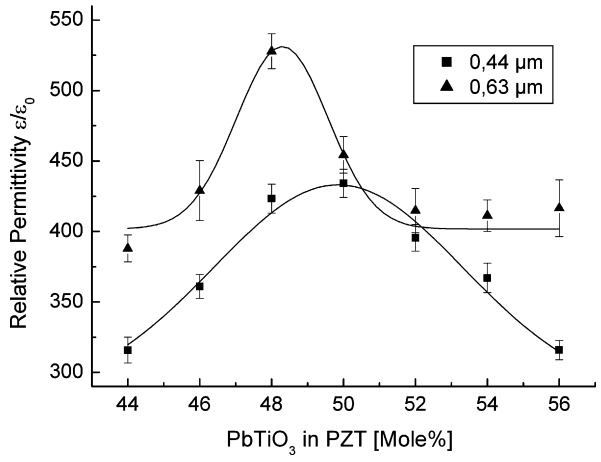


Fig. 6. Relative permittivity (unpolarised) of two Nd–PZT samples with a small grain size. The permittivity peak is shifted towards higher titania content.

The comparison of the shape of the hysteresis loops of a ceramic with large grain size and with small grain size, depicted in Fig. 8, shows a significant difference. Whereas the large grain sized material shows a well defined hysteresis loop, the small grain sized ceramic has only an elliptical hysteresis loop.

### 4.3. Phase content and lattice parameters

The powder diffraction patterns of the large grain sized samples are depicted in Fig. 9. The reflections marked with arrows show clearly the split corresponding to the tetragonal distortion of the perovskite unit cell. Only the sample with a zirconium to titanium ratio of 56/44 shows broad reflections arising from the superposition of the tetragonal and the rhombohedral phases.

In contrast to that, the diffraction patterns of the small grained samples show a significantly different behaviour (Fig. 10). The peak splitting is not as distinctive even for the samples with high titanium content. At lower titanium contents, the reflections become smaller suggesting the presence of only the rhombohedral phase. On a first glance, the coexistence region of the tetragonal and the rhombohedral phases, i.e. the morphotropic

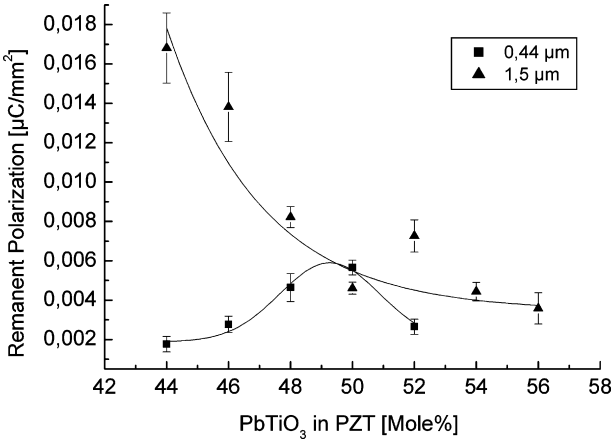


Fig. 7. Comparison of the remanent polarisation (measured at 4 V/µm) of a Nd–PZT sample with a large and a small grain size. The saturation polarisation could not be achieved due to electric breakthrough of the samples.

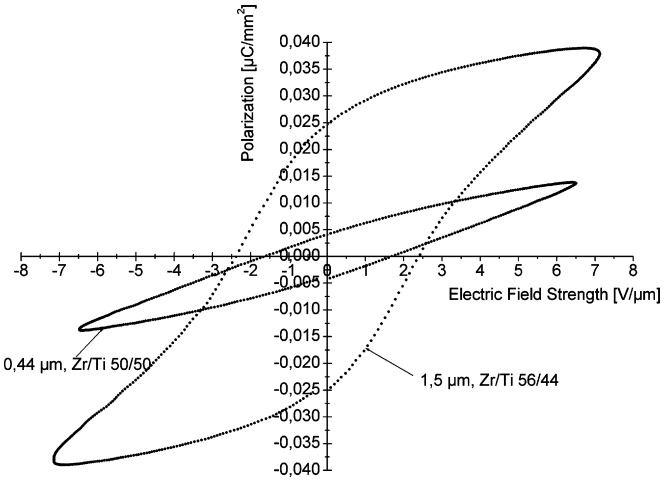


Fig. 8. Comparison of the polarisation–electric field strength hysteresis loops of a Nd–PZT sample with a high and a small grain size.

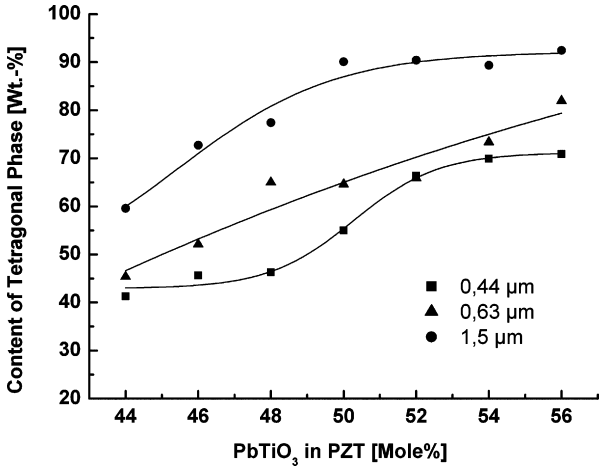


Fig. 11. Quantitative phase content of Nd–PZT samples in dependence of zirconium/titanium ratio and mean grain size.

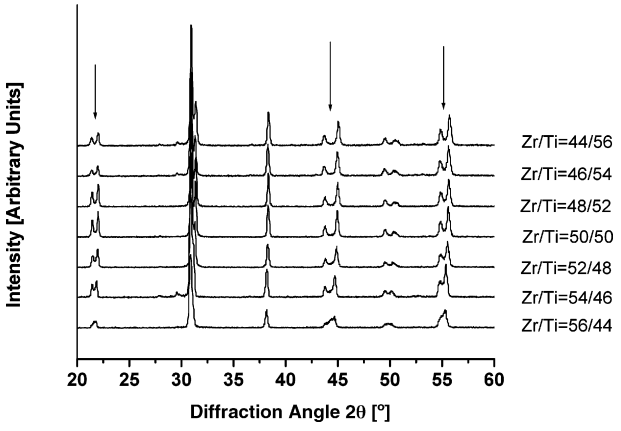


Fig. 9. X-ray diffraction patterns of Nd–PZT ceramics (as sintered) in dependence of the Zr/Ti ratio. The mean grain size of the samples is 1.4 µm. The reflections with a clearly visible peak splitting due to the tetragonal unit cell are marked with arrows.

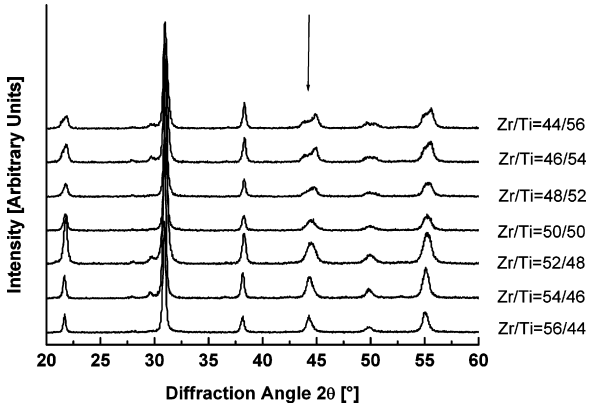


Fig. 10. X-ray diffraction patterns of Nd–PZT ceramics (as sintered) in dependence of the Zr/Ti ratio. The mean grain size of the samples is 0.44 µm. Note the difference to the large grain sized samples. Only the titanium rich samples show a distinct peak splitting.

phase boundary seems to be shifted towards higher titanium contents.

The quantitative phase analysis via the Rietveld refinements confirms this hypothesis. In Fig. 11 the content of the tetragonal phase in dependence of composition and grain size of the NdPZT samples is represented. The results show that the phase boundary is shifted towards higher titanium contents with decreasing grain size. If the position of the morphotropic phase boundary is denoted as the point of equality between the tetragonal and the rhombohedral phase, the MPB shifts from a zirconium/titanium ratio of 56/44 for large grain sizes to 50/50 for a grain size of 0.44 µm.

The results of the refinement of the lattice parameters are illustrated in Fig. 12. The analysis of the lattice parameters of the high grain size samples shows the expected behaviour. Starting from the morphotropic phase boundary, the *c*-axis increases rapidly with increasing titanium content and remains almost equal with further enhancement of titanium content. The *a*-axis

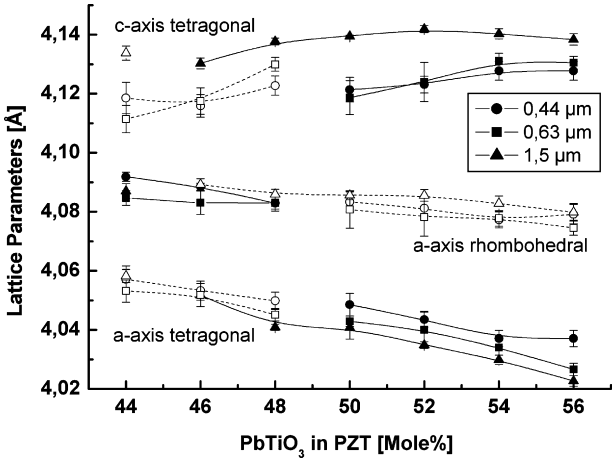


Fig. 12. Lattice parameters of the as sintered samples. The filled symbols represent the parameters of the predominant phase and the open symbols refer to the phase with the lower mass content.

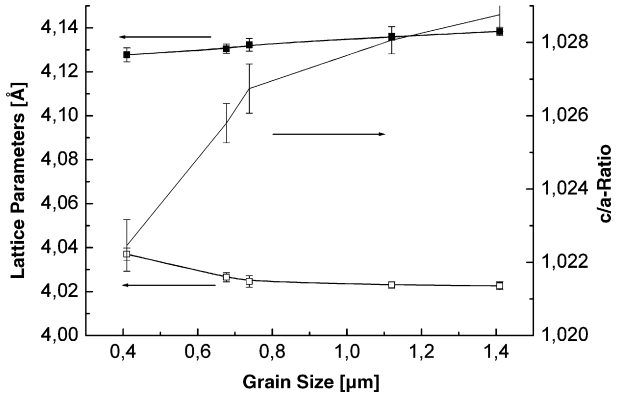


Fig. 13. Lattice parameters and *c*/*a*-ratio of a sample series in the tetragonal range in dependence of the mean grain size.

decreases continuously with higher titanium content. The lattice parameters of the tetragonal phase of the low grain size samples show a similar correlation between unit cell dimensions and chemical composition bearing in mind the shift of the MPB towards higher titanium contents. But compared to the samples with the large grain size, the *c*-axes are significantly compressed whereas the *a*-axes indicate a tendency towards a slight elongation. The lattice parameters measured for a sample series in the titanium rich range depict the compression of the tetragonal unit cell along the *c*-axis and the elongation of the *a*-axis by the reduction of the grain size (Fig. 13). The tetragonal distortion decreases from 1.028 for high grain size samples to 1.023 for low grain sizes.

The comparison of the lattice parameters of as sintered samples with a low grain size and the corresponding ground powders indicates no significant relaxation processes due to grinding. The lattice parameters depicted in Fig. 14 show no increase of the *c*-axis values. Only the *a*-axes seem to be slightly diminished.

A significant change in the phase content after grinding sintered samples could not be observed.

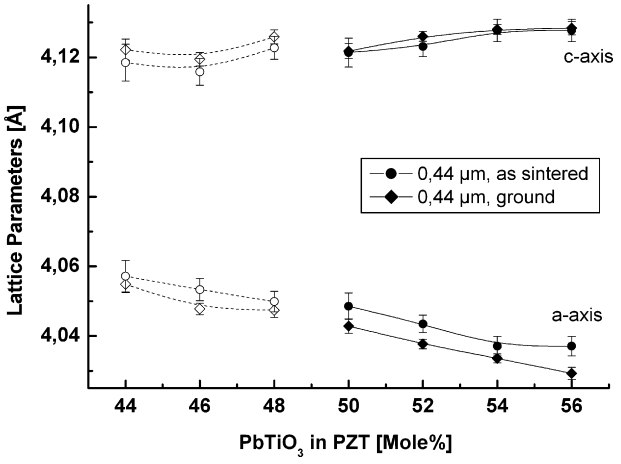


Fig. 14. Comparison between the tetragonal lattice parameters of as sintered disks and ground samples. As an example the sample series with a mean grain size of 0.44 µm was chosen.

## 5. Discussion

### 5.1. Microstructure

The sintering behaviour of the neodymium doped PZT ceramics corresponds to the grain growth characteristics of donor doped PZT published by several authors.[18,19,21,22,43] The maximum grain size of the samples investigated did not exceed 1.7 µm. The grain growth of donor doped PZT during sintering is restricted due to a so-called inhibition effect. An accumulation of the dopants at the grain boundaries is supposed to reduce the grain boundary mobility during sintering.[20] Compared to undoped PZT, the grain size of samples sintered at 1100 °C drops down from 8 µm to 2 µm by the addition of 2 mol% neodymium.[18]

The densification behaviour of donor doped PZT was investigated in detail by Rossner et al.[18] and Hammer and Hoffmann[43] Whereas the grain growth is restricted, the final density of the ceramic can be enhanced by incorporating dopant ions. The detailed sintering characteristics depend on the dopant content and the sintering temperature. The final density increases with the sintering temperature and a shrinkage maximum occurs in the range of 1000–1100 °C.

In correspondence to that, the density of the samples investigated within this study increases with increasing sintering temperature. A closer inspection of the data shows a significantly increased variation of the data at a sintering temperature of 1000 °C and 1100 °C. This fact is likely to be correlated with the shrinkage maximum of neodymium doped PZT in this temperature range. If the sintering process is stopped at this point, small deviations in the process parameters may cause remarkable differences in the microstructure.

### 5.2. Domain configuration

During cooling below the ferroelectric Curie temperature PZT, ceramics undergo a phase transition accompanied by changes in the unit cell dimensions. The resulting internal stress in polycrystalline material is mainly compensated by the formation of ferroelectric domains. The domain size was found to be a function of the mean grain size of the ceramic.[44,45] With decreasing grain size, the characteristic banded structures disappear, the domain size decreases and the domain density increases. The empirical correlation found for barium titanate applies in general for PZT and lead titanate but is not valid in every point. The domain size of extremely fine grained PZT decreases more strongly than expected. Domains smaller than 10 nm were observed in PZT ceramics with a grain size of 150 nm.[45] The domain formation is completely inhibited in 60 nm grains of lead titanate.[46]

We investigated the domain configuration at a sample series with a zirconium to titanium ratio of 46/54, i.e. in the tetragonal composition region. The typical herringbone domain pattern of these samples is in good agreement with the observations of Arlt[44] and Cao and Randall.[45] The granular structures observed at our samples after etching of the small grain size samples are likely related to the very small domains.

We have no definite explanation why domains could not be observed in the high grain size samples at the morphotropic phase boundary. We conclude, that possibly the coexistence between the rhombohedral and the tetragonal phase diminishes the domain size so that they cannot be observed by SEM.

### 5.3. Sample homogeneity

The superior properties of PZT are closely connected with the morphotropic phase boundary, i.e. the composition dependent transition between the tetragonal and the rhombohedral phase. Strictly spoken, this phase boundary in the PZT system is a coexistence range of both phases. The width of the coexistence range is a function of the process parameters. Chemical inhomogeneities can generate a broadening of the range.[2] For the investigation of the correlation of the position of the morphotropic phase boundary and the microstructure, chemical inhomogeneities of the material have to be excluded. But chemical fluctuations in the zirconium–titanium distribution were observed even in ceramics produced via a sol gel process.[47] The reason is a difference in the formation enthalpies of lead titanate and lead zirconate. It was also shown that a preorganisation of Ti–O–Zr chains lowers the activation energy for the formation of PZT.[47] The sol–gel method used for our sample preparation generates such a preorganisation of the Ti–O–Zr chains due to the carboxylation of the alcoholate precursors prior to hydrolysis.[40,48]

### 5.4. Location of the morphotropic phase boundary

The coexistence of the tetragonal and the rhombohedral phase is connected with a significant increase in the dielectric constant and the remanent polarisation of the material. The MPB of PZT ceramics doped with 2 mol% neodymium is located at a zirconium to titanium ratio of 56/44.[7] Our results for the samples with the high grain sizes correspond with these data.

The sample with the lowest zirconium content in our sample series is located at the MPB and thus the values of the dielectric constants and the remanent polarisation decrease with increasing titanium contents.

In contrast to that, the small grain sized samples show a different behaviour. Although the chemical composition is identical to the large grain sized material, the dependence of the dielectric constant and the remanent polarisation show clear peak shapes. This suggests a shift of the morphotropic phase boundary towards higher titanium contents. The shift is more pronounced at smaller grain sizes of the ceramics.

The results from the dielectric and ferroelectric measurements were confirmed by the investigation of the phase content by X-ray diffraction. The ratio between the tetragonal and the rhombohedral phase determined from Rietveld refinements of the data shows a shift of the phase boundary into the titanium rich composition range with decreasing grain size of the ceramics.

The discrepancy of between our results and the data reported in the literature results from the difference in the grain size ranges examined. The mean grain size of about 1 μm seems to be an upper limit for size effects on the morphotropic phase boundary.

Remarkably, the fine grained material shows clamping effects despite a finely distributed pores with sizes in the range of the grain size and a volume fraction up to 25%. One could expect that the pores enable the ceramic grains to relax into the open space.[10] Our observation that the fine grained porous samples show compressed unit cells whereas the dense ceramics with higher grain sizes do not demonstrates that a possible relaxation at grain surfaces does not play a significant role and is not able to compensate clamping occurring within the grains.

As a reason for size effects internal stress is assumed.[7,10] The internal stress emerges from the phase transformation from the cubic high temperature phase to the low temperature phases. In ceramics with sufficiently large grain sizes, the stress is reduced by the formation of domains. As the domain formation is suppressed in low grain size ceramics, the remaining stress increases with decreasing grain size.[49]

The result of internal stress is a deformation of the crystal structure[25] and thus the stability of the phases may be affected.[10] Randall et al. showed that internal stress in low grain size niobium doped PZT ceramics causes a deformation of the tetragonal unit cell. The crystallites are compressed along the *c*-axis.[25] These results correlate well with our findings about the tetragonal phase in the small grain size ceramics. The material with a mean grain size below 1 μm shows a uniaxial compression of the unit cell along the *c*-axis whereas the *a*-axis is slightly elongated. The tetragonal distortion is reduced suggesting directional stress.

As shown in the following model calculations, the directional stress on the tetragonal unit cell is responsible for the destabilisation of the tetragonal phase and the shift of the morphotropic phase boundary towards higher titanium contents.

### 5.5. Model calculations

It was assumed that internal stress is responsible for the destabilisation of the tetragonal phase. We used calculations on the basis of the Devonshire theory to verify our hypothesis. From the compression of the tetragonal *c*-axis and the small elongation of the *a*-axis in the fine grained ceramics was concluded that a compressive stress acts upon the *c*-direction and a smaller tensile stress on the *a*-directions of the unit cell. For the calculations was assumed that the tensile stress is half of the amount of the compressive stress which is a rough estimation of the true values. The rhombohedral phase was assumed to be under compressive stress along the three-fold axis of the unit cell.

We calculated the free energy of the tetragonal and the rhombohedral phase at room temperature under mechanical stress between 0 MPa and 200 MPa based on the following equations using the coefficients published by Amin et al.[38] Adjustments to the influences of the neodymium dopant were not made:

$$G_{\mathrm{rhb}} = (3a_1 - 3Q_{11}X_3 - 6Q_{12}X_3)P_3^2 + 3(a_{11}a_{12})P_3^4 + (3a_{111}6a_{112}a_{123})P_3^6 - 1.5s_{11}^p X_3^2 - 3s_{12}^p X_3^2 \quad (1)$$

$$G_{\mathrm{tet}} = (a_1 - Q_{11}X_3 - 2Q_{12}X_1)P_3^2 + a_{11}P_3^4 + a_{111}P_3^6 - 0.5s_{11}^p(2X_1^2 + X_3^2) - s_{12}^p(X_1^2 + 2X_3X_1) \quad (2)$$

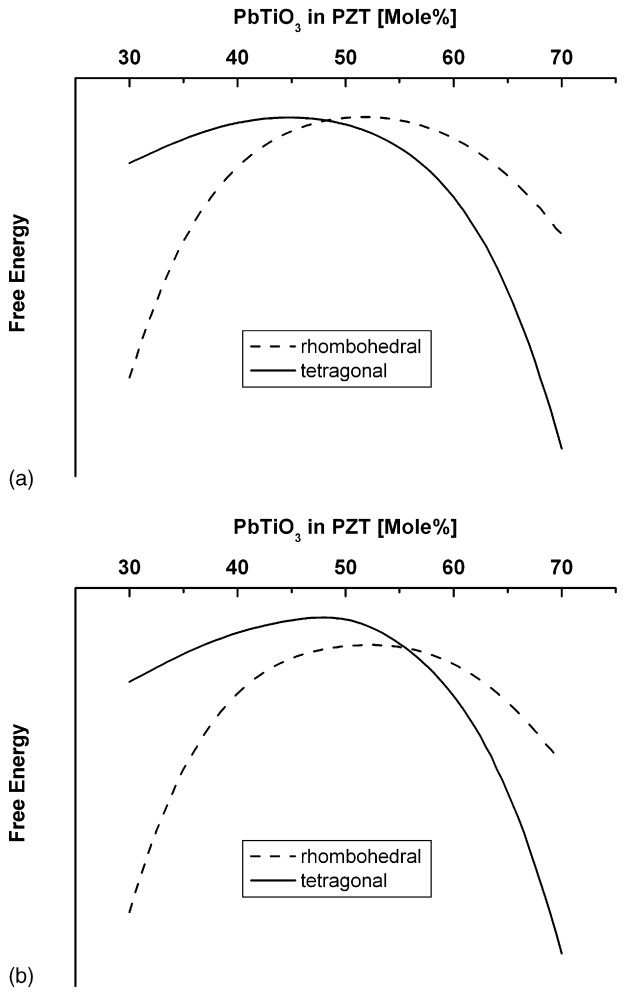


Fig. 15. (a) Free energy of the rhombohedral and the tetragonal phases of PZT at the morphotropic phase boundary, calculated after the Devonshire model for the stress-free case. (b) Free energy of the rhombohedral an the tetragonal phases of PZT at the morphotropic phase boundary, calculated after the Devonshire model. The mechanical stress was set to compression along the *c*-axis and the rhombohedral three-fold axis (50 MPa). A tensile stress was assumed along the *a*-axes of the tetragonal unit cell. The value was set to 25 MPa. Note the shift of the intersection point of the curves in comparison to (a).

The calculations were limited to a section of the phase diagram between 30 mol% and 70 mol% lead titanate. The rhombohedral low temperature phase was not included.

Fig. 15a illustrates the free energy of the tetragonal and the rhombohedral phase for the stress free case. The intersection of the curves represents the position of the morphotropic phase boundary. For the undoped material which is calculated here the boundary is located at 47 mol% lead titanate.

In Fig. 15b, the free energies of the tetragonal and the rhombohedral phase for a compressive stress of 50 MPa is depicted. The free energy of the tetragonal phase increases and thus the intersection point is shifted towards titanium rich compositions. As shown in Fig. 16, the shift of the coexistence point of both phases increases with increasing stress.

The model calculations are in accordance with the experimental observations. As the tetragonal phase elongates in the *c*-direction and contracts in the *a*-direction after the transition to the low temperature phases, directional stress can be assumed. Only a directional stress generates a destabilisation of the tetragonal phase and shifts the MPB towards higher titanium contents whereas a hydrostatic pressure, i.e. an isotropic compression was shown to shift the phase boundary into the opposite direction.[39]

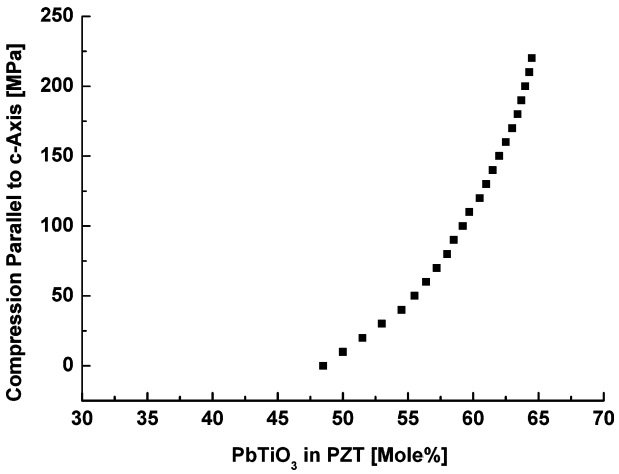


Fig. 16. Position of the morphotropic phase boundary of PZT calculated after the Devonshire model. For the calculation the compressive stress along the tetragonal *c*-axis was accompanied by a compressive stress along the rhombohedral three-fold axis and a tensile stress along the *a*-axes with a value assumed to be half of the compressive stress.

## 6. Conclusion

The investigation of neodymium doped lead zirconate titanate ceramics samples showed that a significant change in the phase stability occurs below a critical grain size of 1 μm. It was found that the morphotropic phase boundary between the rhombohedral and tetragonal phase shifts towards higher titanium contents. The observations are in correspondence with model calculations based on the Devonshire theory. Directional stress is responsible for the destabilisation of the tetragonal phase and thus the MPB is shifted. As a consequence, the material properties of small grain size ceramics like thin films or fine scale fibres can be improved by the adjustment of the chemical composition.

## Acknowledgements

I would like to express my thanks to Dr. Jens Helbig and Prof. Gerd Müller for their support and the inspiring and fruitful discussions. I also thank my co-workers from the Fraunhofer-Institute of Silicate Research (‘Fraunhofer-Institut für Silicatforschung’) for their help with the sample preparation. The research was kindly supported by the German Research Foundation (‘Deutsche Forschungsgemeinschaft’) within the Priority Programme ‘Multifunctional Materials’ (‘Multifunktionswerkstoffe’).

## References

1. Jaffe, B., Roth, R. S. and Marzullo, S., Properties of piezoelectric ceramics in the solid-solution series lead titanate–lead zirconate–lead oxide: tin

oxide and lead titanate–lead hafnate. *J. Res. Natl. Bureau Stand.*, 1955, **55**, 239–254.
2. Kakegawa, K., Mohri, J., Takahashi, T., Yamamura, H. and Shirasaki, S., A compositional fluctuation and properties of $Pb(Zr,Ti)O_3$. *Solid State Commun.*, 1977, **24**, 769–772.
3. Ari-Gur, P. and Benguigui, L., X-ray study of the PZT solid solutions near the morphotropic phase transition. *Solid State Commun.*, 1974, **15**, 1077–1079.
4. Wersing, W., Analysis of phase mixtures in ferroelectric ceramics by dielectric measurements. *Ferroelectrics*, 1974, **7**, 163–165.
5. Ari-Gur, P. and Benguigui, L., Direct determination of the coexistance region in the solid solutions $Pb(Zr_xTi_{1-x})O_3$. *J. Phys. D: Appl. Phys.*, 1975, **8**, 1856–1862.
6. Thomann, H. and Wersing, W., Principles of piezoelectric ceramics for mechanical filters. *Ferroelectrics*, 1982, **40**, 189–202.
7. Wersing, W., Rossner, W., Eckstein, G. and Tomandl, G., The morphotropic phase boundary in PZT ceramics prepared by spray drying of salt solutions and by the mixed oxide method. *Silicates Ind.*, 1985, **3/4**, 41–46.
8. Cao, W. and Cross, E., The ratio of rhombohedral and tetragonal phases on the morphotropic phase boundary in lead zirconate titanate. *Jpn. J. Appl. Phys.*, 1992, **31**, 1399–1402.
9. Cao, W. and Cross, E. L., Theoretical model for the morphotropic phase boundary in lead zirconate–lead titanate solid solution. *Phys. Rev. B*, 1993, **47**, 4825–4830.
10. Härdtl, K. H. and Hennings, D., Wechselwirkungen zwischen Gefüge und Gitterstruktur in der ferroelektrischen Mischkristallreihe $PbTiO_3$–$PbZrO_3$. *Sci. Ceram.*, 1973, **6**, VII/1-VII/15 [in German].
11. Kim, N., Grain size effect on the dielectric and piezoelectric properties in compositions which are near the morphotropic phase boundary of lead zirconate–titanate based ceramics. PhD Thesis. Pennsylvania State University, PA, 1994.
12. Seth, V. K. and Schulze, W. A., Fabrication and characterization of ferroelectric PLZT 7/65/35 ceramic thin films and fibers. *Ferroelectrics*, 1990, **112**, 283–307.
13. Boulton, J. M., Teowee, G. and Uhlmann, D. R., Sol–gel derived PZT fibers. *Mater. Res. Soc. Symp. Proc.*, 1992, **271**, 517–522.
14. Shimono, I., Sugawara, T., Ishimori, F. and Ohara, Y., Preparation of $Pb(Zr_{1-x}Ti_x)O_3$ fibers by the alginate method. *J. Ceram. Soc. Jpn. Int. Ed.*, 1993, **101**, 700–703.
15. Glaubitt, W., Jahn, R. and Merklein, S., Formkörper auf der Basis von PZT ($Pb(Zr,Ti)O_3$), Bleizirkonat-Bleititanat, Verfahren und Zwischenprodukt zu deren Herstellung. German Patent, DE 43 32 831 C1, October 6, 1994 [in German].
16. Watzka, W., Seifert, S., Scholz, H. and Sporn, D., PZT-fiber/polymer composites—preparation and properties. In *Proceedings of the International Conference on Electronic Ceramics & Applications, Electroceramics V, Vol. 1*, 1996, pp. 217–220.
17. Watzka, W., Seifert, S., Scholz, H., Sporn, D., Schönecker, A. and Seffner, L., Dielectric and ferroelectric properties of 1–3 composites containing thin PZT-fibers. In *Proceedings of the 10th IEEE International Symposium on Applications of Ferroelectrics, Vol. II, IEEE Cat. No. 96 CH 35948*, 1996.
18. Rossner, W., Lubitz, K. and Tomandl, G., Densification and crystallite growth in PZT ceramics with variable neodymium content. *Silicates Ind.*, 1985, **3/4**, 31–34.
19. Kulcsar, F., Electromechanical properties of lead titanate zirconate ceramics modified with certain three- or five-valent additions. *J. Am. Ceram. Soc.*, 1959, **42**, 343–349.
20. Atkin, R. B. and Fulrath, R. M., Point defects and sintering of lead zirconate–titanate. *J. Am. Ceram. Soc.*, 1971, **54**, 265–270.
21. Langman, R. A., Runk, R. B. and Butler, S. R., Isothermal grain growth of pressure-sintered PLZT ceramics. *J. Am. Ceram. Soc.*, 1973, **56**, 486–488.
22. Haertling, G. H., Hot-pressed lead zirconate–lead titanate ceramics containing bismuth. *Am. Ceram. Soc. Bull.*, 1964, **43**, 875–879.
23. Webster, A. H. and Weston, T. B., The grain size dependence of the electromechanical properties in lead zirconate–titanate ceramics. *J. Can. Ceram. Soc.*, 1968, **37**, 51–54.
24. Martirena, H. T. and Burfoot, J. C., Grain-size effects on properties of some ferroelectric ceramics. *J. Phys. C: Solid State Phys.*, 1974, **7**, 3182–3192.
25. Randall, C. A., Kim, N., Kucera, J.-P., Cao, W. and Shrout, T. R., Intrinsic and extrinsic size effects in fine-grained morphotropic-phase-boundary lead zirconate titanate ceramics. *J. Am. Ceram. Soc.*, 1998, **81**, 677–688.
26. Surowiak, Z., Kupriyanov, M. F. and Czekaj, D., Properties of nanocrystalline ferroelectric PZT ceramics. *J. Eur. Ceram. Soc.*, 2001, **21**, 1377–1381.
27. Isupov, V. A., Dielectric polarization of $PbTiO_3$–$PbZrO_3$ solid solutions. *Sov. Phys. Solid State*, 1970, **12**, 1084–1088.
28. Wersing, W., Devonshire Betrachtungen zum elastischen Verhalten piezoelektrischer Keramiken. In *Proceedings of the Fourth International Joint Meeting Electron and Magnetoceramics*, 1981, pp. 162–182 [in German].
29. Halemane, T. R., Haun, M. J., Cross, L. E. and Newnham, R. E., A phenomenological theory for phase transitions in perovskite ferroelectrics with oxygen octahedron tilts. *Ferroelectrics*, 1985, **62**, 149–165.
30. Halemane, T. R., Haun, M. J., Cross, L. E. and Newnham, R. E., First order transitions in perovskite ferroelectrics with oxygen octahedron tilts: application to PZT. *Ferroelectrics*, 1986, **70**, 153–159.
31. Amin, A., Cross, L. E. and Newnham, R. E., Calorimetric and phenomenological studies of the $PbZrO_3$:$PbTiO_3$ system. *Ferroelectrics*, 1981, **37**, 647–650.
32. Amin, A., Haun, M. J., Badger, B., McKinstry, H. and Cross, L. E., A phenomenological Gibbs function for the single cell region of the $PbZrO_3$:$PbTiO_3$ solid solution system. *Ferroelectrics*, 1985, **65**, 107–130.
33. Haun, M. J., Furman, E., Jang, S. J. and Cross, L. E., Thermodynamic theory of the lead zirconate–titanate solid solution system. Part I. Phenomenology. *Ferroelectrics*, 1989, **99**, 13–25.
34. Haun, M. J., Zhuang, Z. Q., Furman, E., Jang, S. J. and Cross, L. E., Thermodynamic theory of the lead zirconate–titanate solid solution system. Part III. Curie constant and sixth-order polarization interaction dielectric stiffness coefficients. *Ferroelectrics*, 1989, **99**, 45–54.
35. Haun, M. J., Furman, E., Halemane, T. R. and Cross, L. E., Thermodynamic theory of the lead zirconate–titanate solid solution system. Part IV. Tilting of the oxygen octahedral. *Ferroelectrics*, 1989, **99**, 55–62.
36. Haun, M. J., Furman, E., Jang, S. J. and Cross, L. E., Thermodynamic theory of the lead zirconate–titanate solid solution system. Part V. Theoretical calculations. *Ferroelectrics*, 1989, **99**, 63–86.
37. Yamamoto, T. and Makino, Y., Pressure dependence of ferroelectric properties in $PbZrO_3$–$PbTiO_3$ solid state system under hydrostatic stress. *Jpn. J. Appl. Phys.*, 1996, **35**(Part I, 5B), 3214–3217.
38. Amin, A., Newnham, R. E. and Cross, L. E., Effect of elastic boundary conditions on morphotropic $Pb(Zr,Ti)O_3$ piezoelectrics. *Phys. Rev. B*, 1986, **34**, 1595–1598.
39. Oh, S. H. and Jang, H. M., Three-dimensional phase diagram of the $Pb(Zr,Ti)O_3$ system under hydrostatic pressure. *Ceram. Int.*, 2000, **26**, 565–569.
40. Ahlfänger, R., Bertagnolli, H., Ertel, T., Kolb, D., Peter, D., Naß, R. *et al.*, First evidence of the preformation of an inorganic network in sol–gel processing of lead zirconate titanate, obtained by EXAFS spectroscopy. *Ber. Bunsenges. Phys. Chem.*, 1991, **95**, 1286–1289.
41. Bruggemann, D. A. G., Berechnung verschiedener physikalischer Konstanten von heterogenen Substanzen. I. Dielektrizitätskonstanten und Leitfähigkeitender Mischkörper aus isotropen Substanzen. *Ann. Phys.*, 1935, **24**, 636–679 [in German].
42. Roßner, W., Sinterverhalten und elektrische Eigenschaften von Neodym dotierter Bleizirkonat-Titanat-Keramik, hergestellt nach dem Mixed-Oxide-Verfahren. PhD Thesis. Erlangen-Nürnberg, Germany, 1985 [in German].
43. Hammer, M. and Hoffmann, M. J., Sintering model for mixed-oxide-derived lead zirconate titanate ceramics. *J. Am. Ceram. Soc.*, 1998, **81**, 3277–3284.
44. Arlt, G., The influence of microstructure on the properties of ferroelectric ceramics. *Ferroelectrics*, 1990, **104**, 217–227.
45. Cao, W. and Randall, C. A., Grain size and domain size relations in bulk ceramic ferroelectric materials. *J. Phys. Chem. Solids*, 1996, **57**, 1499–1505.

46. Ren, S., Lu, C., Liu, J., Shen, H. and Wang, Y., Size-related ferroelectric-domain-structure transition in a polycrystalline $PbTiO_3$ thin film. *Phys. Rev. B*, 1996, **54**, 14337–14340.
47. Bertagnolli, H. and Merkle, R., Investigation of the crystallization of lead titanate and lead zirconate titanate with X-ray diffraction and differential thermal analysis. *Ber. Bunsenges.*, 1998, **102**, 1023–1031.
48. Glaubitt, W., Sporn, D. and Jahn, R., Sol–gel processing of PZT long fibers. In *Advances in Science and Technology, Vol. 10: Intelligent Materials and Systems*, ed. P. Vincenzini. Techna Faenza, 1995, pp. 47–54.
49. Burggraf, A. J. and Keizer, K., Effects of microstructure an the dielectric properties of lanthana substituted $PbTiO_3$ and $Pb(Zr,Ti)O_3$–ceramics. *Mater. Res. Bull.*, 1975, **10**, 521–528.